Method to integrate full particle orbit in toroidal plasmas

X. S. Wei[1], Y. Xiao[1,*], A. Kuley[2] and Z. Lin[2]
[1]Institute for Fusion Theory and Simulation, Zhejiang University
[2]University of California, Irvine
*yxiao@zju.edu.cn

Abstract

It is important to integrate full particle orbit accurately to a long time in tokamaks when studying charged particle dynamics in electromagnetic waves with frequency higher than the cyclotron frequency. We derive the form of the Boris scheme using magnetic coordinates, which can be used effectively for long time scale integration of the cyclotron orbit in toroidal plasmas. The new method has been verified in a toroidal simulation with the absence of the high frequency waves. The full particle orbit calculation recovers the guiding center banana orbit. This method has better numeric properties than the conventional Runge-Kutta method in conserving particle energy and magnetic moment. The toroidal precession frequency is found to match that from the guiding center simulation. Many other important physics phenomena, such as the $E \times B$ drift, the Ware pinch effect and the neoclassical polarization drift are also verified by the full orbit simulation.

I. Introduction

Particle-in-cell (PIC) simulation is widely used to study the complicated plasma dynamics,[1] where the position and velocity of the charged particles as well as the electromagnetic fields are advanced in time simultaneously. Pushing particle in the phase space is an essential part of the PIC simulation. In order to simulate the particle motion in the slowly varying electromagnetic fields (with frequency lower than the cyclotron frequency), the formulation to push the guiding centers in magnetic coordinates has been developed and greatly advanced the gyrokinetic simulation. [2-5] When the electromagnetic field frequency is comparable or higher than the cyclotron frequency, e.g., the radio frequency (RF) electromagnetic waves used for plasma heating, the full particle orbit instead of the guiding center orbit needs to be calculated accurately to a very long time scale.[6-9]

Boris algorithm is an outstanding choice to integrate the cyclotron orbit of the charged particle with its explicit nature.[10, 11] Although it is not symplectic, this algorithm conserves the phase space volume as has recently been discovered, making it very attractive in the long-time simulation.[12, 13] The conventional Boris algorithm works well in the Cartesian coordinates. However, the magnetic coordinates are more suited to describe the complicated magnetic geometry and electromagnetic fluctuations in the toroidal plasmas. Therefore it is desirable to work out a Boris scheme in the magnetic coordinates to accommodate the physics complexity in the magnetic fusion devices like

tokamaks. In addition, this algorithm should be able to handle the long time scale particle dynamics, which can be testified by the known particle dynamics with the low frequency waves.

In this paper we derive the form of the Boris scheme in the magnetic coordinates which is used effectively to push particles to the long time scale in the toroidal plasmas. In Section II, the basic Boris scheme is introduced and the magnetic coordinates are used to advance the particle position in the Boris scheme. The complication in advancing velocity in magnetic coordinates is carefully examined in Section III. Section IV shows simulation verification results based on the new Boris formulation, including the bounce motion and toroidal precession of the banana orbits, the $E \times B$ drift, the Ware pinch effect and neoclassical polarization drift in the absence of high frequency waves. Summary and discussion are provided in Section V.

II. Boris algorithm and position advance in toroidal system

The motion of a charged particle in the electromagnetic field is given by:

$$\frac{d\mathbf{x}}{dt} = \mathbf{v} \tag{1}$$

$$\frac{d\mathbf{v}}{dt} = \frac{e}{m}\left(\mathbf{E} + \mathbf{v} \times \mathbf{B}\right) \tag{2}$$

The leap-frog method has been widely used to advance this equation by shifting the position and velocity of the particle by $\Delta t / 2$ to make the scheme time-centered::

$$\frac{\mathbf{x}^{t+\Delta t/2} - \mathbf{x}^{t-\Delta t/2}}{\Delta t} = \mathbf{v}^{t} \tag{3}$$

$$\frac{\mathbf{v}^{t+\Delta t} - \mathbf{v}^{t}}{\Delta t} = \frac{e}{m}\left(\mathbf{E} + \frac{\mathbf{v}^{t+\Delta t} + \mathbf{v}^{t}}{2} \times \mathbf{B}\right) \tag{4}$$

In Eq.(4), the electric field $\mathbf{E}$ and magnetic field $\mathbf{B}$ are evaluated at the time of $t + \Delta t / 2$. In addition, Eq.(4) is implicit in nature. So advancing **v** is relatively troublesome. However, Boris introduced two intermediate velocities $\mathbf{v}^{-}$ and $\mathbf{v}^{+}$ to make Eq.(4) explicit. These two intermediate velocities connect with $\mathbf{v}^{t}$ and $\mathbf{v}^{t+\Delta t}$ respectively through the following equations

$$\mathbf{v}^{-} = \mathbf{v}^{t} + \frac{e\Delta t}{2m}\mathbf{E} \tag{5}$$

$$\mathbf{v}^{+} = \mathbf{v}^{t+\Delta t} - \frac{e\Delta t}{2m}\mathbf{E} \tag{6}$$

Thus the acceleration effect of the electric field $\mathbf{E}$ is split into two half accelerations. Between these two half accelerations, the velocity vector $\mathbf{v}^{+}$ at the time step $t + \Delta t/2$ can be obtained from $\mathbf{v}^{-}$ by the following vector rotation:

$$\frac{\mathbf{v}^{+} - \mathbf{v}^{-}}{\Delta t} = \frac{e}{m}\left(\frac{\mathbf{v}^{+} + \mathbf{v}^{-}}{2} \times \mathbf{B}\right), \tag{7}$$

which approximates the Lorentz rotation in the magnetic field. We note that the preceding equation is still in the implicit form. However, it can be further transformed to the following explicit form.[10]

$$\mathbf{v}^{+}=\mathbf{v}^{-}+\left(\mathbf{v}^{-}+\mathbf{v}^{-}\times\mathbf{t}\right)\times\mathbf{s} \tag{8}$$

with $\mathbf{t}=\frac{\Omega\Delta t}{2}\mathbf{b},\mathbf{s}=\frac{\Omega\Delta t}{1+\left(\Omega\Delta t/2\right)^{2}}\mathbf{b}$, the gyrofrequency $\Omega=\frac{eB}{m}$, and the unit vector along the magnetic field $\mathbf{b}=\frac{\mathbf{B}}{B}$. Here the symbol e denotes the particle charge. Therefore, the procedure of advancing velocity is separated into three steps: half-acceleration by the electric field, rotation by the magnetic field, and another half-acceleration by the electric field. In the Cartesian coordinates, with $\mathbf{v}=v_x\mathbf{e}_x+v_y\mathbf{e}_y+v_z\mathbf{e}_z$, the time advancing of velocity is straightforward by following Eqs.(5), (6) and (8) in the three fixed orthogonal directions.

For a toroidal system like tokamak, it is usually more convenient to use magnetic flux coordinates $\left(\psi,\theta,\zeta\right)$ rather than the Cartesian coordinates, where $2\pi\psi$ is the poloidal magnetic flux, ζ and θ are the effective toroidal and poloidal angle respectively. In the gyrokinetic description, the velocity $\mathbf{v}$ is decomposed into three components: $v_{\parallel}$, μ and the phase angle φ, where φ is an ignorable variable due to the fast gyromotion. Therefore the guiding center of the particle is pushed in the 5D phase space $\left(\psi,\theta,\zeta,v_{\parallel},\mu\right)$ by the guiding center equation of motion, which can be derived from the guiding center Hamiltonian principle [2]. In the full-kinetic simulation, this decomposition of the velocity variable to $\left(v_{\parallel},\mu,\varphi\right)$ will lead to numerical difficulties since these variables are defined on a local orthogonal coordinate system which rotates with the particle motion and hence is not fixed in time and space, e.g., the phase angle will rotate along the magnetic field line in a sheared magnetic field even without any particle gyromotion.

The velocity $\mathbf{v}$ is then decomposed into three covariant basis vectors $\mathbf{e}_i=\frac{d\mathbf{r}}{d\alpha_i}$, with $\alpha_i=\psi,\theta,\zeta$ for $i=1,2,3$, which can be defined by the magnetic coordinates. Then $\mathbf{v}=(v^{\psi},v^{\theta},v^{\zeta})=\sum_{i=1}^{3}v^{\alpha_i}\mathbf{e}_i$, with the contravariant velocity component $v^{\alpha_i}=\mathbf{v}\cdot\nabla\alpha_i$ The contravariant basis vector is defined as $\mathbf{e}^{i}=\nabla\alpha_i$, with $\mathbf{e}^{i}=J^{-1}\varepsilon_{ijk}\mathbf{e}_j\times\mathbf{e}_k$, where ε_{ijk} is the Levi-Civita symbol, $\varepsilon_{ijk}=1$ if the indices $\left(i,j,k\right)$ follow an even permutation of $\left(1,2,3\right)$;

$\varepsilon_{ijk} = -1$ if the indices (i, j, k) follow an odd permutation of $(1,2,3)$; otherwise $\varepsilon_{ijk} = 0$. The transformation Jacobian J between the covariant form and contravariant form is $J = \mathbf{e}_1 \times \mathbf{e}_2 \cdot \mathbf{e}_3$, and $J^{-1} = \mathbf{e}^1 \times \mathbf{e}^2 \cdot \mathbf{e}^3$. The position advance in the magnetic flux coordinates derived from Eq.(3) takes the form

$$\alpha_i{}^{t+\Delta t/2} = \alpha_i{}^{t-\Delta t/2} + v^{\alpha_i} t \Delta t \tag{9}$$

Once the new particle position $\alpha_i{}^{t+\Delta t/2}$ is known, the contravariant basis vector $\mathbf{e}^{it+\Delta t/2}$ at this new time step can be computed.

In the following section we show how to evolve from $\mathbf{v}^t$ to $\mathbf{v}^{t+\Delta t}$ in the magnetic flux coordinates according to the Boris algorithm.

III. Advance velocity in toroidal systems

Since the particle changes its position with time, the basis vectors $\mathbf{e}^i$ and $\mathbf{e}_i$ at the particle position also change with time. In the absence of inductive field, the electric field can be derived from the electrostatic potential $\mathbf{E} = -\nabla\phi$. The velocity evolution equation in Boris scheme, i.e., Eqs. (5) and (6), can be projected to the three contravariant basis vectors $\mathbf{e}^{it+\Delta t/2}$ for $i = 1,2,3$ at the new time step $t + \Delta t/2$. Define $u^{\alpha_i t} = \mathbf{v}^t \cdot \mathbf{e}^{it+\Delta t/2}$, $u^{\alpha_i t+\Delta t} = \mathbf{v}^{t+\Delta t} \cdot \mathbf{e}^{it+\Delta t/2}$, $u^{\alpha_i -} = \mathbf{v}^- \cdot \mathbf{e}^{it+\Delta t/2}$ and $u^{\alpha_i +} = \mathbf{v}^+ \cdot \mathbf{e}^{it+\Delta t/2}$, then Eqs. (5) and (6) can be rewritten as

$$u^{\alpha_i -} = u^{\alpha_i t} - \frac{\Omega \Delta t}{2B} \sum_{j=1}^{3} \frac{\partial \phi}{\partial \alpha_j} g^{\alpha_j \alpha_i} \tag{10}$$

$$u^{\alpha_i t+\Delta t} = u^{\alpha_i +} - \frac{\Omega \Delta t}{2B} \sum_{j=1}^{3} \frac{\partial \phi}{\partial \alpha_j} g^{\alpha_j \alpha_i} \tag{11}$$

where the geometric tensor $g^{\alpha_j \alpha_i} = \mathbf{e}^{jt+\Delta t/2} \cdot \mathbf{e}^{it+\Delta t/2}$. If not mentioned explicitly, these geometric tensors in the following are evaluated at time step $t + \Delta t/2$. Similarly, we can define the geometric tensor $g_{\alpha_i \alpha_j} = \mathbf{e}_i \cdot \mathbf{e}_j$ and $g_{\alpha_i}^{\alpha_j} = \mathbf{e}_i \cdot \mathbf{e}^j$. The contravariant component of Eq.(8) gives

$$u^{\alpha_i +} = u^{\alpha_i -} + \mathbf{v}^- \times \mathbf{s} \cdot \mathbf{e}^{it+\Delta t/2} + \left(\mathbf{v}^- \times \mathbf{t}\right) \times \mathbf{s} \cdot \mathbf{e}^{it+\Delta t/2} \tag{12}$$

Suppose that the magnetic field in toroidal system can be expressed in both covariant or

contravariant form,[2] $\mathbf{B} = \delta\nabla\psi + I\nabla\theta + g\nabla\zeta = q\nabla\psi\times\nabla\theta + \nabla\zeta\times\nabla\psi$, where $q = q(\psi)$ is the safety factor, $\delta = \delta(\psi,\theta)$, $I = I(\psi)$ and $g = g(\psi)$. Thus the magnetic field can also be written in terms of the basis vectors defined before:

$$\mathbf{B} = \sum_{j=1}^{3} B_j \mathbf{e}^j = \sum_{i=1}^{3} B^i \mathbf{e}_i \tag{13}$$

with $B_j = (\delta, I, g)$, $B^i = \left(0, J^{-1}, q(J)^{-1}\right)$ and the Jacobian $J = \dfrac{qg+I}{B^2}$. With these notations, Eq. (12) can be further simplified as

$$\begin{aligned} u^{\alpha_i +} = \left[1 - \frac{\gamma_B}{2}(\Omega\Delta t)^2\right] u^{\alpha_i -} + \gamma_B \frac{(\Omega\Delta t)^2}{2B^2} \sum_{j=1}^{3} B^i B_j u^{\alpha_j -} \\ - \frac{\gamma_B}{J}\frac{\Omega\Delta t}{B} \sum_{j,k,l=1}^{3} \varepsilon_{ijl} B_j g_{\alpha_k \alpha_l} u^{\alpha_k -} \end{aligned} \tag{14}$$

with the constant $\gamma_B = \dfrac{1}{1+(\Omega\Delta t)^2/4}$. This equation can be explicitly expressed for each component in the following way:

$$u^{\psi +} = \left[1 - \frac{\gamma_B}{2}(\Omega\Delta t)^2\right] u^{\psi -} + \frac{\gamma_B}{J}\frac{\Omega\Delta t}{B} \sum_{k=1}^{3} \left(g g_{\alpha_k \theta} - I g_{\alpha_k \zeta}\right) u^{\alpha_k -} \tag{15}$$

$$\begin{aligned} u^{\theta +} = \left[1 - \frac{\gamma_B}{2}(\Omega\Delta t)^2\right] u^{\theta -} + \gamma_B \frac{(\Omega\Delta t)^2}{2B^2}\frac{1}{J}\left(\delta u^{\psi -} + I u^{\theta -} + g u^{\zeta -}\right) \\ + \frac{\gamma_B}{J}\frac{\Omega\Delta t}{B} \sum_{k=1}^{3} \left(\delta g_{\alpha_k \zeta} - g g_{\alpha_k \psi}\right) u^{\alpha_k -} \end{aligned} \tag{16}$$

$$\begin{aligned} u^{\zeta +} = \left[1 - \frac{\gamma_B}{2}(\Omega\Delta t)^2\right] u^{\zeta -} + \gamma_B \frac{(\Omega\Delta t)^2}{2B^2}\frac{q}{J}\left(\delta u^{\psi -} + I u^{\theta -} + g u^{\zeta -}\right) \\ + \frac{\gamma_B}{J}\frac{\Omega\Delta t}{B} \sum_{k=1}^{3} \left(I g_{\alpha_k \psi} - \delta g_{\alpha_k \theta}\right) u^{\alpha_k -} \end{aligned} \tag{17}$$

The preceding equations can be used to compute $u^{\alpha_i +}$ ($i = 1,2,3$), which then can be further used to compute $u^{\alpha_i t+\Delta t}$ using Eq.(11). However, $v^{\alpha_i t+\Delta t}$ instead of $u^{\alpha_i t+\Delta t}$ is required to evolve $\alpha_i^{\,t+\Delta t/2}$ to $\alpha_i^{\,t+3\Delta t/2}$, with $v^{\alpha_i t+\Delta t} = \mathbf{v}^{t+\Delta t}\cdot\mathbf{e}^{it+\Delta t}$. The basis vector $\mathbf{e}^{it+\Delta t} = \nabla\alpha_i^{\,t+\Delta t}$ remains unknown since $\alpha_i^{\,t+\Delta t}$ has not been evaluated in the Boris scheme. Here we use an estimate for $\alpha_i^{\,t+\Delta t}$:

$$\alpha_i^{t+\Delta t} = \alpha_i^{t+\Delta t/2} + u^{\alpha_i t+\Delta t}\frac{\Delta t}{2} \tag{18}$$

Once $\alpha_i^{t+\Delta t}$ is known, then $v^{\alpha_i t+\Delta t}$ can be calculated by

$$v^{\alpha_i t+\Delta t} = \sum_{j=1}^{3} u^{\alpha_j t+\Delta t}\mathbf{e}_j^{\,t+\Delta t/2}\cdot\mathbf{e}^{it+\Delta t} \tag{19}$$

Thus the new position is given by $\alpha_i^{t+3\Delta t/2} = \alpha_i^{t+\Delta t/2} + v^{\alpha_i t+\Delta t}\Delta t$, for $i = 1,2,3$, according to Eq.(12) . Then the velocity variable $\tilde{u}^{\alpha_i t+\Delta t}$ in the next step of velocity evolution needs to know the basis vector $\mathbf{e}^{i\,t+3\Delta t/2}$ rather than $\mathbf{e}^{i\,t+\Delta t/2}$, which can be then obtained by

$$\tilde{u}^{\alpha_i t+\Delta t} = \sum_{j=1}^{3} u^{\alpha_j t+\Delta t}\mathbf{e}_j^{\,t+\Delta t/2}\cdot\mathbf{e}^{it+3\Delta t/2} \tag{20}$$

With the preceding steps, we can advance one full time step in the original Boris scheme. However, in Eqs.(19), (20) we need to calculate the dot product of the covariant and contravariant basis vectors at different time steps. It is mostly convenient for this calculation once we know the transform between $(\alpha_1,\alpha_2,\alpha_3)$ and the Cartesian coordinates (x,y,z) , since $\mathbf{e}^i = \frac{\partial\alpha_i}{\partial x}\hat{\mathbf{x}} + \frac{\partial\alpha_i}{\partial y}\hat{\mathbf{y}} + \frac{\partial\alpha_i}{\partial z}\hat{\mathbf{z}}$ and $\mathbf{e}_i = \frac{\partial x}{\partial\alpha_i}\hat{\mathbf{x}} + \frac{\partial y}{\partial\alpha_i}\hat{\mathbf{y}} + \frac{\partial z}{\partial\alpha_i}\hat{\mathbf{z}}$. Note the unit vectors $(\hat{\mathbf{x}},\hat{\mathbf{y}},\hat{\mathbf{z}})$ do not change with the particle motion. It is often more convenient to introduce an intermediate toroidal coordinate system $(\beta_i)=(R,Z,\phi)$, and find the transformation between the magnetic flux coordinates (α_i) and the toroidal coordinates (β_i) first. The transformation between (β_i) and (x,y,z) is straightforward. Then we can rewrite Eq.(19) and Eq.(20) in a more specific form

$$u^{\alpha_i,\text{new}} = \sum_{j=1}^{3}\sum_{m=1}^{3}\sum_{n=1}^{3} u^{\alpha_j,\text{old}}\left(\frac{\partial x}{\partial\beta_m}\frac{\partial\beta_m}{\partial\alpha_j},\frac{\partial y}{\partial\beta_m}\frac{\partial\beta_m}{\partial\alpha_j},\frac{\partial z}{\partial\beta_m}\frac{\partial\beta_m}{\partial\alpha_j}\right)\cdot\left(\frac{\partial\alpha_i}{\partial\beta_n}\frac{\partial\beta_n}{\partial x},\frac{\partial\alpha_i}{\partial\beta_n}\frac{\partial\beta_n}{\partial y},\frac{\partial\alpha_i}{\partial\beta_n}\frac{\partial\beta_n}{\partial z}\right) \tag{21}$$

It is interesting to know that Eq.(19) and Eq.(20) can be regarded as a rotation of the basis vectors as the particle position changes from one time step to the next time step. Therefore in a locally orthogonal system, the transformation can be greatly simplified. For example, we can find the transformation analytically in the limit of concentric circular cross section, which is a very useful equilibrium model for many applications. When a particle moves from $(\psi_1,\theta_1,\zeta_1)$ to $(\psi_2,\theta_2,\zeta_2)$, the directions of the basis vectors change with time as shown in Fig. 1. This rotation can be separated into three steps: a first rotation about ζ axis by an angle $-\theta_1$, a second

rotation about θ' axis by an angle $\Delta\zeta = \zeta_2 - \zeta_1$, a third rotation about the ζ'' axis by an angle θ_2. Thus the initial basis vectors can be written by the linear sum of the final ones:

$$\begin{aligned}\mathbf{e}_{\psi}^{\text{old}} = \Big\{ & \mathbf{e}_{\psi}^{\text{new}} \left|\nabla\psi_2\right| \left[\sin\theta_1 \sin\theta_2 + \cos\theta_1 \cos\theta_2 \cos\Delta\zeta\right] + \\ & \mathbf{e}_{\theta}^{\text{new}} \left|\nabla\theta_2\right| \left[\sin\theta_1 \cos\theta_2 - \cos\theta_1 \sin\theta_2 \cos\Delta\zeta\right] - \mathbf{e}_{\zeta}^{\text{new}} \left|\nabla\zeta_2\right| \sin\Delta\zeta \cos\theta_1 \Big\} \frac{1}{\left|\nabla\psi_1\right|}\end{aligned} \tag{22}$$

$$\begin{aligned}\mathbf{e}_{\theta}^{\text{old}} = \Big\{ & \mathbf{e}_{\psi}^{\text{new}} \left|\nabla\psi_2\right| \left[\cos\theta_1 \sin\theta_2 - \sin\theta_1 \cos\theta_2 \cos\Delta\zeta\right] \\ & + \mathbf{e}_{\theta}^{\text{new}} \left|\nabla\theta_2\right| \left[\cos\theta_1 \cos\theta_2 + \sin\theta_1 \sin\theta_2 \cos\Delta\zeta\right] + \mathbf{e}_{\zeta}^{\text{new}} \left|\nabla\zeta_2\right| \sin\Delta\zeta \sin\theta_1 \Big\} \frac{1}{\left|\nabla\theta_1\right|}\end{aligned} \tag{23}$$

$$\mathbf{e}_{\zeta}^{\text{old}} = \left[\mathbf{e}_{\psi}^{\text{new}} \left|\nabla\psi_2\right| \cos\theta_2 \sin\Delta\zeta - \left|\nabla\theta_2\right| \mathbf{e}_{\theta}^{\text{old}} \sin\theta_2 \sin\Delta\zeta + \left|\nabla\zeta_2\right| \mathbf{e}_{\zeta}^{\text{old}} \cos\Delta\zeta \right] \frac{1}{\left|\nabla\zeta_1\right|} \tag{24}$$

The velocity does not change with the basis vectors, i.e.

$$\mathbf{v} = \sum u^{i,\text{old}} \mathbf{e}_i^{\text{old}} = \sum u^{i,\text{new}} \mathbf{e}_i^{\text{new}} \tag{25}$$

The new components of velocity can then be written as

$$\begin{aligned}u^{\psi,\text{new}} = \left|\nabla\psi_2\right| \Bigg[& \frac{u^{\psi,\text{old}}}{\left|\nabla\psi_1\right|} \left(\sin\theta_1 \sin\theta_2 + \cos\theta_1 \cos\theta_2 \cos\Delta\zeta\right) \\ & + \frac{u^{\theta,\text{old}}}{\left|\nabla\theta_1\right|} \left(\cos\theta_1 \sin\theta_2 - \sin\theta_1 \cos\theta_2 \cos\Delta\zeta\right) + \frac{u^{\zeta,\text{old}}}{\left|\nabla\zeta_1\right|} \cos\theta_2 \sin\Delta\zeta \Bigg]\end{aligned} \tag{26}$$

$$\begin{aligned}u^{\theta,\text{new}} = \left|\nabla\theta_2\right| \Bigg[& \frac{u^{\psi,\text{old}}}{\left|\nabla\psi_1\right|} \left(\sin\theta_1 \cos\theta_2 - \cos\theta_1 \sin\theta_2 \cos\Delta\zeta\right) \\ & + \frac{u^{\theta,\text{old}}}{\left|\nabla\theta_1\right|} \left(\cos\theta_1 \cos\theta_2 + \sin\theta_1 \sin\theta_2 \cos\Delta\zeta\right) - \frac{u^{\zeta,\text{old}}}{\left|\nabla\zeta_1\right|} \sin\theta_2 \sin\Delta\zeta \Bigg]\end{aligned} \tag{27}$$

$$u^{\zeta,\text{new}} = \left|\nabla\zeta_2\right| \left[-\frac{u^{\psi,\text{old}}}{\left|\nabla\psi_1\right|} \cos\theta_1 \sin\Delta\zeta + \frac{u^{\theta,\text{old}}}{\left|\nabla\theta_1\right|} \sin\theta_1 \sin\Delta\zeta + \frac{u^{\zeta,\text{old}}}{\left|\nabla\zeta_1\right|} \cos\Delta\zeta \right] \tag{28}$$

The preceding three equations can be used to compute the $v^{\alpha_i t+\Delta t}$ and $\tilde{u}^{\alpha_i t+\Delta t}$ in the Eq.(19) and (20) respectively for a concentric circular cross section tokamak. For other non-circular cross section tokamaks, one needs to resort to Eq. (21) for a general treatment.

IV. Simulation Results

The new algorithm is implemented in a full kinetic code and is being incorporated to the gyrokinetic particle simulation code GTC. Several simulations of the charged particle orbit in

tokamaks are carried out to demonstrate the validity and usefulness of this new Boris algorithm in magnetic coordinates. The typical orbits for trapped and passing particles are shown in the left panels of Fig.2. The right panels show the poloidal projection of the particles on the R-Z plane. The full particle trajectories are closed on themselves on the R-Z plane after several hundreds of gyroperiods as predicated by the analytical theory, which indicates good numerical conservation properties for this new algorithm. Although there is a coordinate transformation in every time step, this new algorithm does not lose accuracy in the long time scale.

As a comparison, the 4th order Runge-Kutta algorithm (RK4) is also employed to simulate particle orbit in the tokamak. Fig.3 shows the time history for the kinetic energy E_k and magnetic moment μ for Boris algorithm and RK4 respectively, where the kinetic energy $E_k = \frac{1}{2}mv^2$ and magnetic moment $\mu = \frac{mv_\perp{}^2}{2B}$ are calculated from the velocity of the particle and local geometrical information at each time step. As seen in Fig. 3, for the same time step size $\Delta t = 1/32T_c$ with $T_c = 2\pi/\Omega$, the RK4 algorithm fails to conserve kinetic energy and magnetic moment, while Boris algorithm conserves kinetic energy and magnetic moment over one thousand gyroperiods. In fact, since the magnetic field is static, only the direction of the particle velocity changes at each time step in the Boris scheme, which leads to a perfect conservation of the kinetic energy. The magnetic moment μ in long time simulation shows variation in three different time scales. Firstly in the fastest time scale, the magnetic moment oscillates with the gyromotion. Secondly, the magnetic moment oscillates in the slower bounce time scale. Thirdly, in the even longer time scale the magnetic moment decreases very slowly due to the numerical dissipation.

To test the convergence of this algorithm, we carry out several simulations for different time step sizes. We plot in Fig.4 the motion of the particle in toroidal direction. When $\Delta t = 1/32T_c$, the black solid curve denoting the Boris algorithm coincides with the cyan dashed curve denoting the RK4 algorithm, which means that these methods converge to the exact particle orbit in the small time step size limit as is expected. The RK4 curve begins to deviate from the converged one when $\Delta t = 1/16T_c$ and gives a diverged orbit when $\Delta t = 1/8T_c$. However, it is surprising to see that the Boris algorithm maintains adequate accuracy even when $\Delta t = 1/8T_c$. If there are high frequency electromagnetic perturbations, $\omega_{perturbation}\Delta t < 1$ sets an upper bound for the time step.

We also simulate the guiding center orbits with the same initial parameters. As Fig. 5(a) shows, the guiding center orbit does not match exactly the full particle orbit. Although the same equilibrium magnetic field is used in the guiding center orbit simulation and full particle orbit simulation, there still unavoidably exists some higher order correction in the ε expansion due the different formulations for these two algorithms, where ε is the inverse aspect ratio and $\varepsilon \equiv r/R_0$. The

difference for the bounce time of a trapped particle between these two simulation methods is calculated and plotted in Fig. 5(b). If the equilibrium magnetic field in guiding center simulation and full particle simulation is accurate to the first order of ε, the difference is found proportional to the order of ε^2. This result shows that the difference between the guiding center and full particle orbits is much smaller than the implementation difference of the equilibrium model. In addition, the toroidal precession of trapped particles[14, 15] is investigated using both full particle and guiding center simulations. Fig. 6(a) shows toroidal angle versus time. The slope of the local maxima gives the toroidal precession speed, which can be used to compute the toroidal precession frequency. The toroidal precession frequencies for different pitch angles are shown in Fig. 6(b) with the normalized pitch angle $\lambda=\mu B_0/\varepsilon_k$, and B_0 the magnetic field at the magnetic axis, where the continuous curves are from full particle simulation and the discrete circles are from the guiding center simulation. The results from these two methods are consistent with each other, which verifies the ∇B drift and the curvature drift in the Boris scheme, and shows the effectiveness of the Boris algorithm in the very long time scale simulation. With an external poloidal electric field added, the particle will possess a radial $E\times B$ drift. The $E\times B$ drift is verified in Fig. 7.

If there is a toroidal electric field, the Ware pinch[16] can be recovered by the Boris full particle simulation. As illustrated in Fig.8 (a), the projection of the orbit on the R-Z plane is no longer closed and there is a radial drift with the speed $v = E_\phi / B_p$. The radial drift speed of the trapped particle can also be calculated by its orbit, as shown in Fig. 8(b), which matches the theoretical prediction. If a time-dependent radial electric field is introduced, there will be a radial drift proportional to $\frac{\partial E_r}{\partial t}$ given by $v_p = \frac{\varepsilon_0}{ne}\frac{\omega_{pi}^2}{\omega_{ci}^2}\frac{\partial E_r}{\partial t}\frac{B_0^2}{B_p^2}$, which is the neoclassical polarization drift.[17] If a monotonically increasing electric field is applied, i.e. $E_r(t) = E_0 t$, a constant radial drift v_p is observed, as shown in Fig.9 (b). This neoclassical polarization drift can also be computed from the full particle orbit, which matches the theoretical prediction.

V. Summary

In this paper, we have derived the form of the Boris algorithm in the magnetic coordinates to push full particle (i.e., with cyclotron motion) orbits in the toroidal plasmas. The geometric tensor and Jacobian both appear in the equations of motions to advance the position and velocity, which need to be calculated at the beginning of the simulation. The contravariant component of the velocity needs to be recalculated at each step to advance the velocity since the basis vectors change at the particle position change as the particle moves. This new algorithm is implemented to calculate the full particle orbit of the charged particle in a tokamak, showing faithfully the bounce motion and toroidal precession in a long time scale. The kinetic energy and magnetic moment of

particle are well conserved in this new algorithm.

The orbit from the full particle simulation by the Boris algorithm coincides with the orbit from the guiding center simulation. Although more computation time is needed for the Boris full particle pushing algorithm compared with the guiding center pushing algorithm, this Boris algorithm is still desirable since it can treat properly the crucial wave-particle interaction in the high frequency RF heating scenarios. With low frequency external perturbation fields, this new Boris algorithm can faithfully recover the well-known physics including toroidal precession, Ware pinch and neoclassical polarization. Finally we note that this method and formulation work well not only for the magnetic coordinate system, but also for any other curvilinear coordinate system, such as the widely used toroidal coordinates (R, Z, ϕ).

Acknowledgments

The work is supported by the National Magnetic Confinement Fusion Science Program under Grant No. 2011GB105001, 2013GB111000 and No. 2015GB110000, China NSFC under Grant No. 91130031, the Recruitment Program of Global Youth Experts, US DOE SciDac GSEP centers. The authors thank Professor Liu Chen for useful discussions.

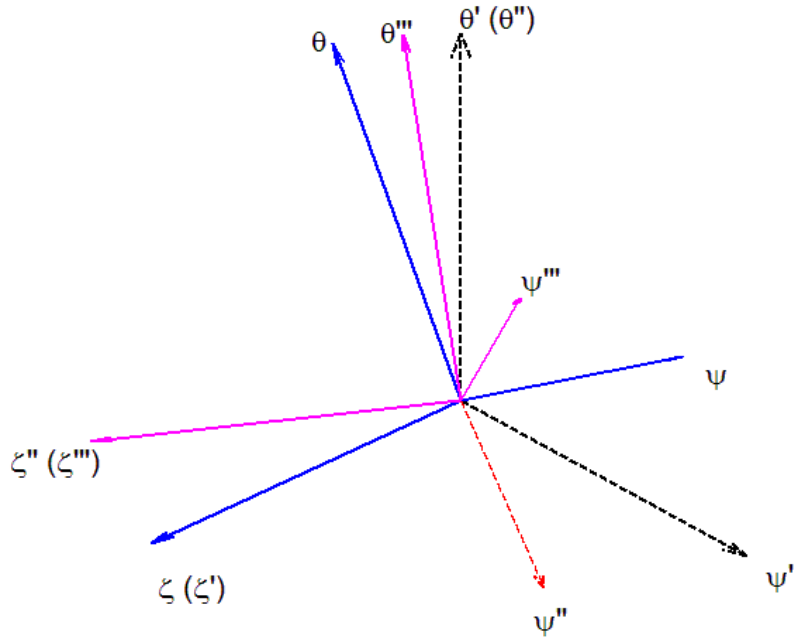

Figure 1: The rotation of unit basis vectors: $\left(\hat{\psi},\hat{\theta},\hat{\zeta}\right)$ is the initial direction of three unit vectors; $(\hat{\psi}',\hat{\theta}',\hat{\zeta}')$ is the three unit vectors after the first rotation; $(\hat{\psi}'',\hat{\theta}'',\hat{\zeta}'')$ is the three unit vectors after the second rotation; $(\hat{\psi}''',\hat{\theta}''',\hat{\zeta}''')$ is the three unit vectors after the third rotation.

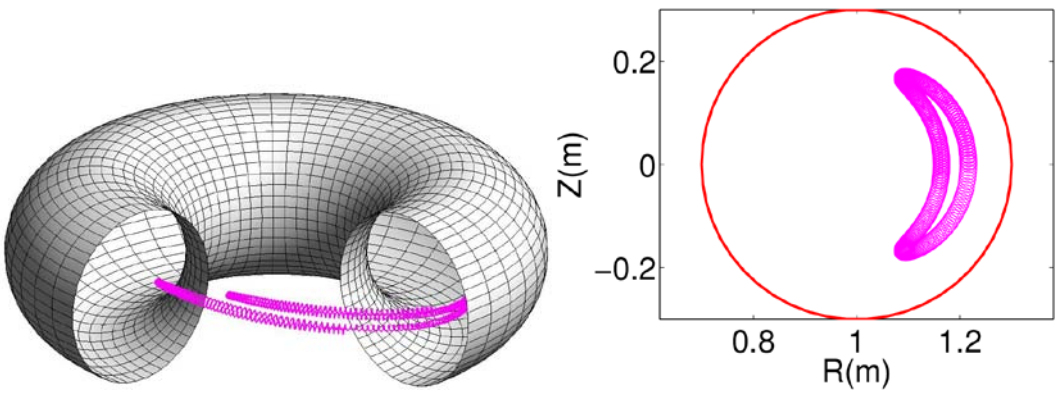

(a) (b)

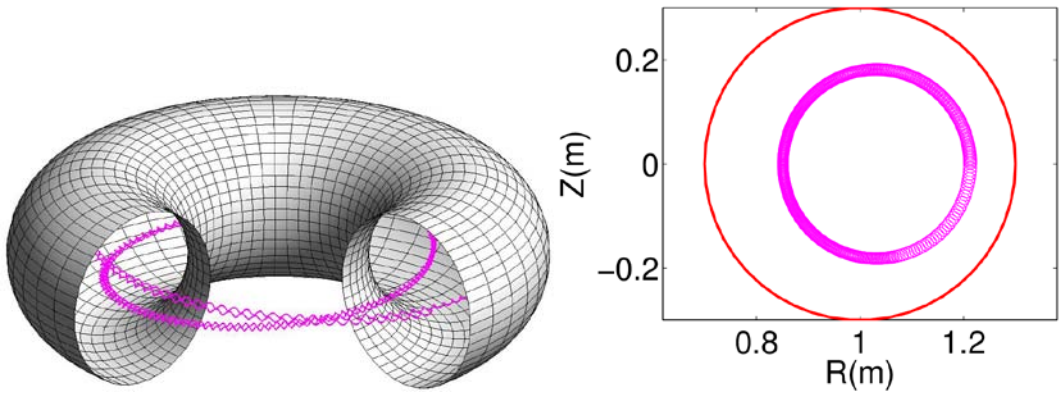

(c) (d)

Figure 2: (a) Orbit of a trapped particle in the tokamak. (b) Projection of the trapped orbit on the R-Z plane (c) Orbit of a passing particle. (d) Projection of the passing orbit on the R-Z plane. The projection is closed during several banana or transit periods.

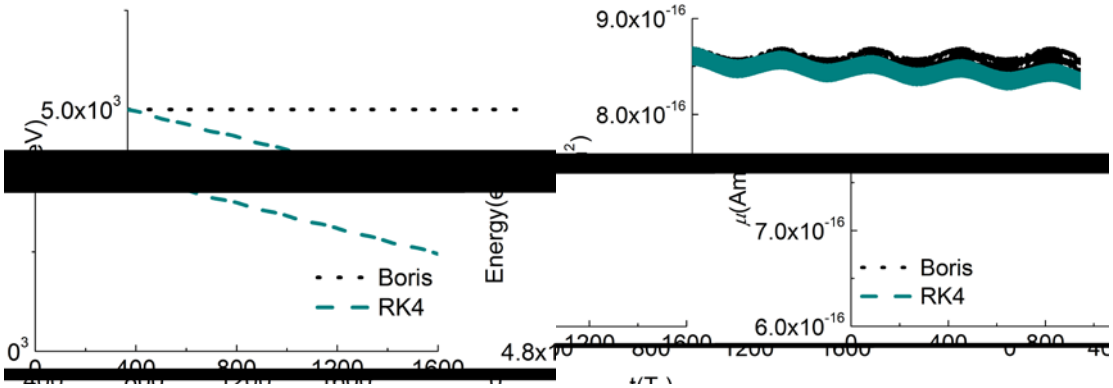

(a) (b)

Figure 3: (a) Time history of the kinetic energy of a particle for the Boris algorithm and the four-order Runge-Kutta algorithm (RK4). (b) Time history of the magnetic moment of the particle for the Boris algorithm and RK4 algorithm. The width of the line shows the fluctuation caused by gyro-motion. The simulations last for about four bounce periods.

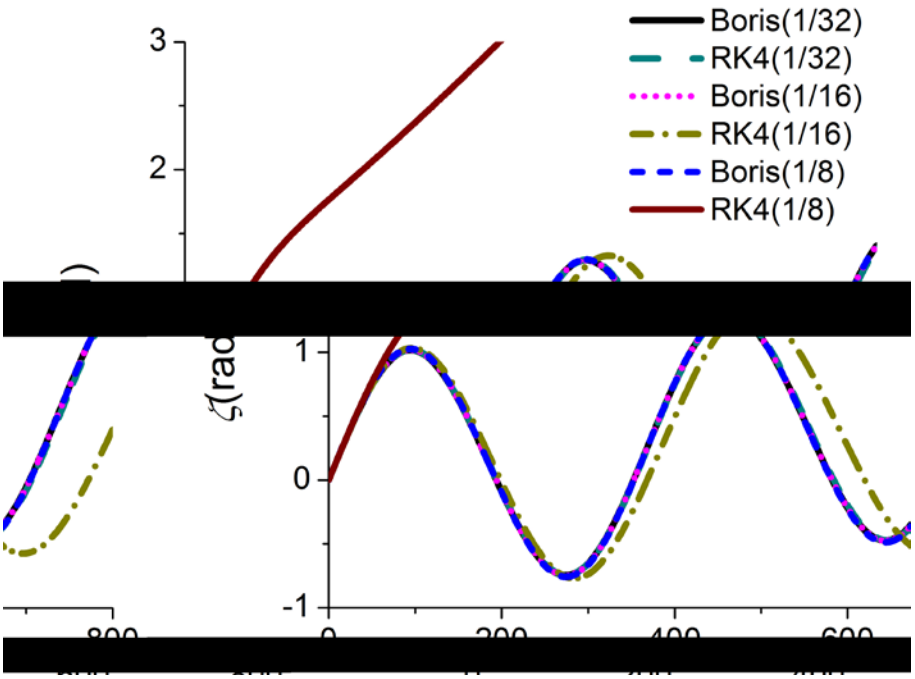

Figure 4: Time history of the toroidal angle of the particle with different sizes of time step.

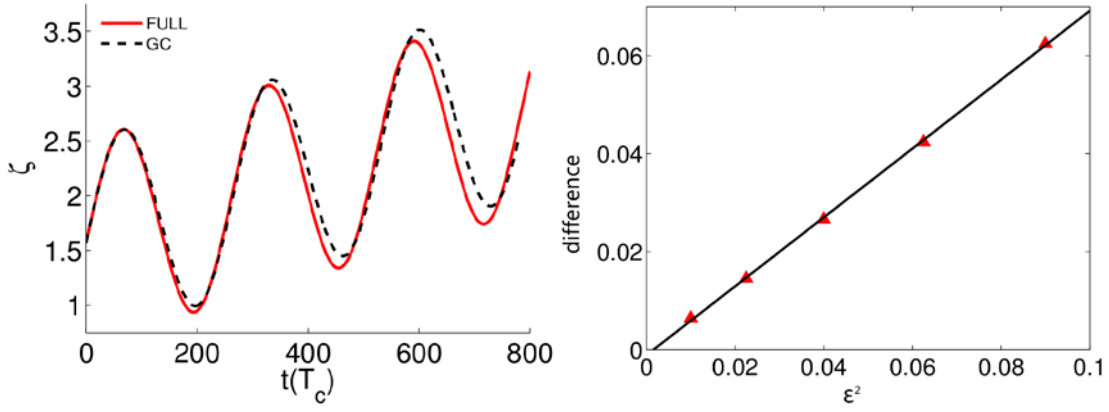

(a) (b)

Figure 5: (a) Time history of the toroidal angle of a trapped particle for full particle(FULL) simulation and guiding center(GC) simulation. (b) The relative difference for the bounce time between the full kinetic simulation and the guiding center simulation. The red markers are from the simulation data, and the black line is a fitted straight line.

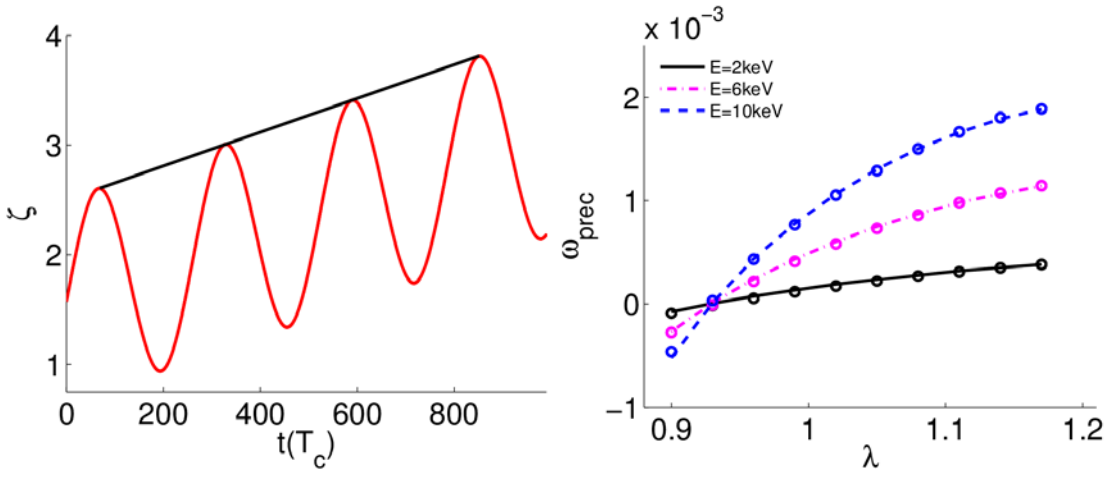

(a) (b)

Figure 6: (a) Calculation of the toroidal precession frequency. The red curve shows the toroidal angle of a trapped particle. The black solid line connects several local maxima, i.e., the banana tips. Then the slope of the black solid line is the toroidal precession frequency. (b) The toroidal precession frequency of trapped particles vs pitch angle for different energies: the continuous curves with different colors are from the full particle orbit simulation by the Boris algorithm, and the discrete circular markers are from the guiding center simulation.

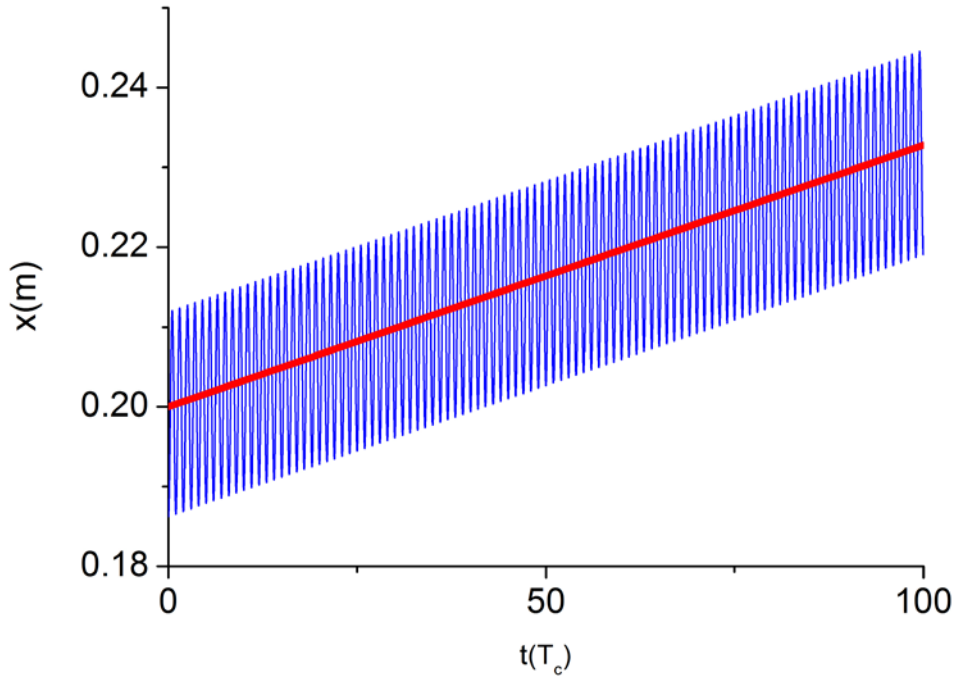

Figure 7: The motion of a particle in the direction of $\mathbf{E}\times\mathbf{B}$ drift. The blue line is the position of the particle in simulation. The red line is the average drift predicted by theory.

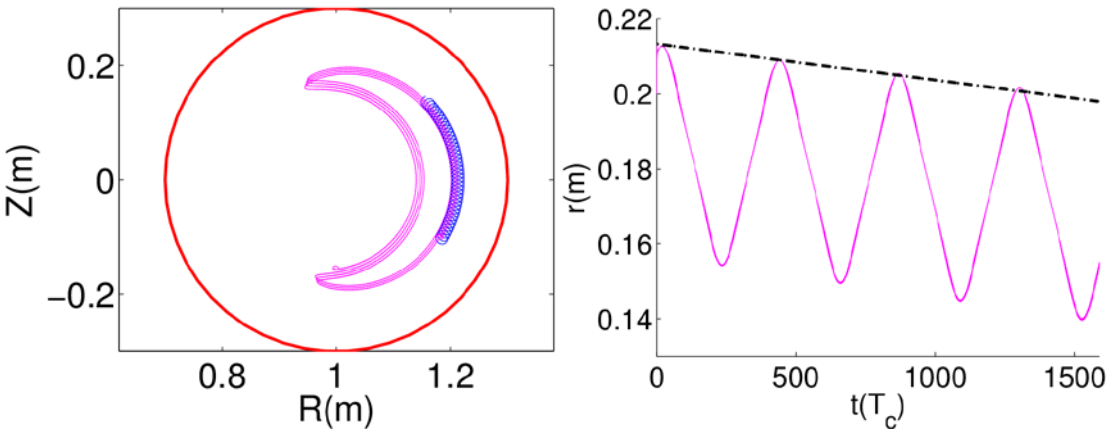

(a) (b)

Figure 8: (a) Ware pinch due to the presence of toroidal electric field. The magenta solid line is the gyrocenter orbit after smoothing out the particle gyromotion in the full particle simulation. The blue line stands for the particle orbit for the beginning time steps. (b) The radial motion of gyrocenter (magenta solid line) and the black line is the radial drift predicted by the Ware pinch theory.

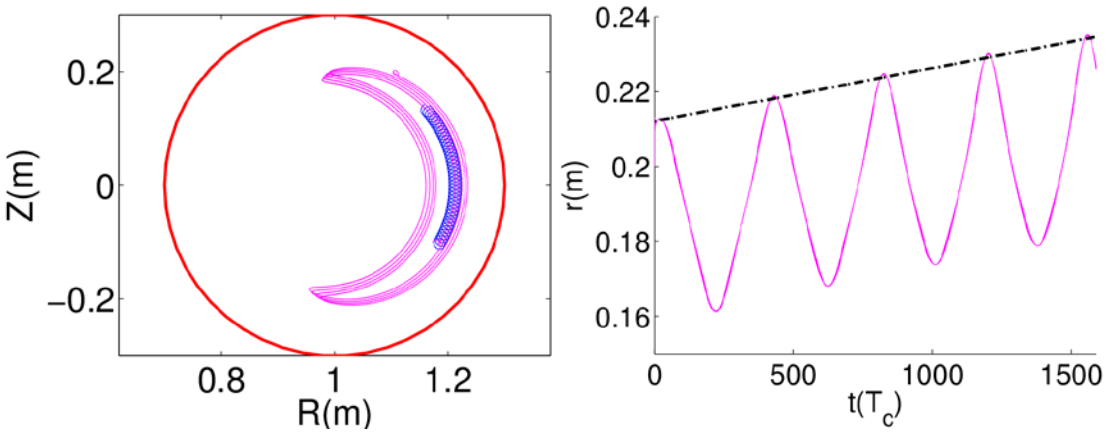

(a) (b)

Figure 9: (a) Neoclassical polarization drift due to increasing radial electric field. The magenta solid line stands for the gyrocenter orbit after smoothing out the particle gyromotion in the full particle simulation. The blue solid line stands for the particle orbit for the beginning time steps. (b) Radial motion of gyrocenter(magenta line) and the black line is the neoclassical polarization drift predicted by theory.

Reference

1. C. K. Birdsall and A. B. Langdon, *Plasma Physics via Computer Simulation*. (CRC Press, 2004).
2. R. B. White and M. S. Chance, Physics of Fluids **27** (10), 2455-2467 (1984).
3. W. W. Lee, Physics of Fluids **26** (2), 556-562 (1983).
4. H. Qin and X. Guan, Physical Review Letters **100** (3) (2008).
5. Z. Lin, T. S. Hahm, W. W. Lee, W. M. Tang and R. B. White, Science **281** (5384), 1835-1837 (1998).
6. A. Kuley, Z. X. Wang, Z. Lin and F. Wessel, Physics of Plasmas **20** (10), 1063 (2013).
7. Y. Lin, X. Y. Wang, Z. Lin and L. Chen, Plasma Physics and Controlled Fusion **47** (4) (2005).
8. Y. Lin, X. Y. Wang, L. Chen, X. Lu and W. Kong, Plasma Physics and Controlled Fusion **53** (5) (2011).
9. Y. Chen and S. E. Parker, Physics of Plasmas **16** (5) (2009).
10. J. P. Boris, in *Proc. Fourth Conf. Num. Sim. Plasmas, Naval Res. Lab, Wash. DC* (1970), pp. 3-67.
11. L. Patacchini and I. H. Hutchinson, Journal of Computational Physics **228** (7), 2604-2615 (2009).
12. H. Qin, S. Zhang, J. Xiao, J. Liu, S. Yajuan and W. M. Tang, Physics of Plasmas **20** (8) (2013).
13. G. L. Delzanno and E. Camporeale, Journal of Computational Physics **253** (2013).
14. A. J. Brizard, Physics of Plasmas **18** (2) (2011).
15. Y. Xiao and Z. Lin, Physics of Plasmas **18** (11), 110703 (2011).
16. A. A. Ware, Physical Review Letters **25** (1) (1970).
17. Y. Xiao, P. J. Catto and W. Dorland, Physics of Plasmas **14** (5) (2007).